ISSN 0015-4628, Fluid Dynamics, 2014, Vol. 49, No. 6, pp. 804–818. © Pleiades Publishing, Ltd., 2014.
Original Russian Text © M.A. Zubin, F.A. Maksimov, N.A. Ostapenko, 2014, published in Izvestiya Rossiiskoi Akademii Nauk, Mekhanika Zhidkosti i Gaza, 2014, Vol. 49, No. 6, pp. 118–134.

Distinctive Features of the Shock Layer Flow Structure in Conical Gas Flows

M. A. Zubin, F. A. Maksimov, and N. A. Ostapenko

Institute of Mechanics, Lomonosov Moscow State University,
Michurinskii pr. 1, Moscow, 119192 Russia
e-mail: zubinma@mail.ru, f_a_maximov@mail.ru, ostap@imec.msu.ru

Received December 10, 2008

Abstract—The results of a numerical and experimental investigation of the flow structure in symmetric and nonsymmetric flows around V-wings with attached shocks on the leading edges are presented. Emphasis is placed on the appearance of new critical points, including vortex Ferri singularities, in the shock layer and transformations in the flow structure with increase in the angles of attack and yaw. In particular, it is established that the flow structure in the plane of symmetry of the flow around V-wings without yaw, which involves the Mach-type shock configuration, undergoes a jumpwise variation with increase in the angle of attack. Additionally to one Ferri singularity of the node type located at the corner point of the transverse wing contour in the plane of symmetry of the flow, there arise two more critical points, those of flow divergence and convergence. The latter point is the second Ferri singularity; it is located nearer to the bridge-shaped shock of the Mach-type shock system and can be of both the node and the saddle type. In the latter case there appear two vortex Ferri singularities located at the vertices of the contact discontinuities proceeding from this critical point on both sides of the plane of symmetry. Certain data on the position of the critical points relative to the wing contour bend are presented as functions of the wing geometry, together with the transformation of the topological shock-layer flow pattern in the presence of yaw. The comparison of the results calculated within the framework of the Euler model with the experimental data on the shock-layer flow structure obtained using a special optical method for visualizing conical flows showed their good agreement.

Keywords: supersonic flows, V-wing, conical flows, Mach-type shock configuration, vortex Ferri singularities.

DOI: 10.1134/S001546281406012X

The existence of flow regimes with Ferri singularities floating above the windward side of V-wings in the plane of symmetry of the flow in the presence of a Mach-type shock configuration was first noticed in [1, 2]. The same studies describe the cases in which internal shocks proceed from triple points; they belong to the weak family and admit the branching into two shocks of the strong family, of which one is incident on the wing wall, while the other hits the contact discontinuity proceeding from the branching point of the bow shock. When the branching of the weak internal shock cannot occur, the supersonic region behind it is closed by a submerging shock. At the times, when the above-mentioned studies had been published, the possibilities of the computery did not make it possible to use high-resolution computation grids. For this reason, certain inferences made in [1, 2] were though true but only qualitative. This concerns with the treatment of the flow structure on the axis of symmetry in the shock layer which was made on the basis of the pressure distributions along the axis of symmetry and over the wing surface and the constant-entropy contours (streamlines) which, owing to an inadequate accuracy of the calculations, did not allow one to determine the flow direction in the vicinity of the central chord of the wing. New possibilities of the computational technologies in connection with the problem under consideration were demonstrated with reference to a certain succession of the regimes of flow around V-wings, in particular, in [3] but the authors of that study did not made a necessary analysis of the flow structure and the factors generating it.

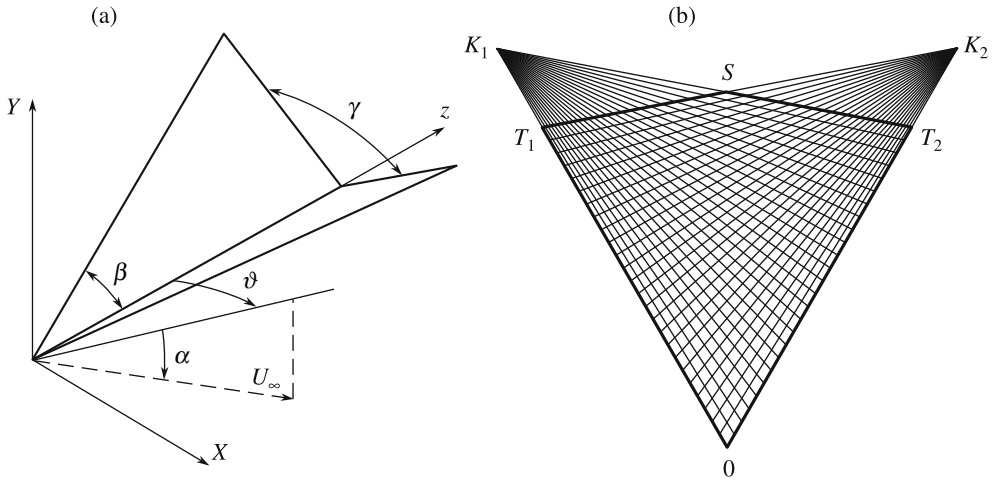

Fig. 1. V-wing in the Cartesian coordinate system; γ and β are the angles of vee and wing vertex and α and ϑ are the angles of attack and yaw (a); computation grid for calculating flow between the wing panels (b).

Below, on the basis of the developed second-order computational code, we present certain results [4] of the calculations of symmetric and nonsymmetric flows around V-wings of different geometry at the Mach number M = 3 and moderate yaw angles and compare the results with the experimental data obtained using direct-shadow optical method for visualizing supersonic conical flows [5]. A time-dependent method was used on special grids with the boundary conditions which took account for the characteristic properties of the disturbed flow in the vicinity of the leading edges of the wings of different geometries with attached shocks.

1. METHOD OF SOLUTION

In the generalized coordinate system the system of Euler equations for calculating conical flows takes the form:

$$\frac{\partial}{\partial t}\frac{\mathbf{U}}{J} + \frac{\partial}{\partial \xi}\frac{\mathbf{E}^*}{J} + \frac{\partial}{\partial \eta}\frac{\mathbf{F}^*}{J} = -2\frac{\mathbf{G}}{J}, \tag{1.1}$$

$$\mathbf{E}^* = \xi_x(\mathbf{E} - \xi\mathbf{G}) + \xi_y(\mathbf{F} - \eta\mathbf{G}), \qquad \mathbf{F}^* = \eta_x(\mathbf{E} - \xi\mathbf{G}) + \eta_y(\mathbf{F} - \eta\mathbf{G}),$$

$$\mathbf{U} = \begin{Bmatrix} \rho \\ \rho u \\ \rho v \\ \rho w \\ \rho e \end{Bmatrix}, \quad \mathbf{E} = \begin{Bmatrix} \rho u \\ \rho u^2 + p \\ \rho uv \\ \rho uw \\ (\rho e + p)u \end{Bmatrix}, \quad \mathbf{F} = \begin{Bmatrix} \rho v \\ \rho uv \\ \rho v^2 + p \\ \rho vw \\ (\rho e + p)v \end{Bmatrix}, \quad \mathbf{G} = \begin{Bmatrix} \rho w \\ \rho uw \\ \rho vw \\ \rho w^2 + p \\ (\rho e + p)w \end{Bmatrix}.$$

In Eq. (1.1) t is time, ρ is the density, (u, v, w) are the velocity $\mathbf{V}$ vector components in the (x, y, z) directions of the Cartesian coordinate system (Fig. 1), p is the pressure, and e is the internal energy of the perfect gas.

The dimensionless variables are determined in accordance with the formulas

$$\rho = \frac{\rho'}{\rho'_\infty}, \qquad p = \frac{p'}{p'_\infty}, \qquad \mathbf{X} = \frac{\mathbf{X}'}{L'}, \qquad \mathbf{V} = \mathbf{V}'\left(\frac{p'_\infty}{\rho'_\infty}\right)^{-1/2}. \tag{1.2}$$

In Eqs. (1.2) the primes denote the dimensional quantities, while the subscript ∞ refers to the values of the corresponding parameters in the freestream. Here L' is the scale length, $\mathbf{X} = (x, y, z)$, and $\mathbf{V} = (u, v, w)$.

The self-similar variables $\xi = x/z$, $\eta = y/z$, and $\zeta = z$ are introduced. It is assumed that the z axis coincides with the central chord of the wing (Fig. 1a).

The generalized coordinates are introduced as follows: $\xi = \xi(x, y)$, $\eta = \eta(x, y)$, and $\zeta = z$. It is assumed that the flow possesses the conical symmetry which is equivalent to the condition $\mathbf{U}_\zeta = 0$.

In the $z = 1$ section the system of Euler equations takes the form (1.1). The metric coefficients and the transformation Jacobian are calculated for a given gridpoint distribution in the physical space in accordance with the formulas

$$\xi_x = J \cdot y_\eta, \quad \xi_y = -J \cdot x_\eta, \quad \eta_x = -J \cdot y_\xi, \quad \eta_y = J \cdot x_\xi, \quad J^{-1} = x_\xi \cdot y_\eta - x_\eta \cdot y_\xi.$$

We will consider flow regimes with shocks attached to the leading edges of a V-wing. To calculate the flow between its panels having swept leading edges the computation grid is constructed by the set of points of intersection between the lines K_1T_2 and K_2T_1 (Fig. 1b). The coordinate lines of the same direction are determined by the trace of the leading edge K_1 of the left panel of the wing in the $z = 1$ plane (one gridpoint of the coordinate lines) and the points uniformly located on the opposite panel from the corner point O to a certain point T_2. The position of point T_2 is preassigned in the vicinity of the trace of the second leading edge K_2 so that the corresponding coordinate line passes only through the regions of the undisturbed flow or the uniform flow behind the plane shock attached to the right leading edge. The coordinate lines of the second direction relate the trace of the right leading edge K_2 with the points on the left panel from the corner point O to a certain point T_1, whose position is given in accordance with the requirements for point T_2. The gridpoints of the computation grid are determined by the points of intersection of the corresponding coordinate lines.

The impermeability condition is imposed on two boundaries OT_1 and OT_2 of the computation domain OT_1ST_2O located on the wing surface (Fig. 1b), while the condition of the flow "conicity" with respect to points K_1 and K_2 is preassigned at two opposite boundaries ST_1 and ST_2. This is permissible, since the wing panels are plane and the traces of the shocks attached to the leading edges coincide with certain coordinate lines proceeding from points K_1 and K_2. The conditions in the undisturbed flow are preassigned only at point S. This formulation of the problem furnishes certain advantages in the numerical modeling which are due to the fact that sharp edges, in which nonunique values of the gasdynamic parameters are realized, are excluded from consideration. Moreover, the analytical solution of the problem of flow past a wedge is not fixed on the boundaries, this solution in any case differing from that obtained on the difference grid owing to special features of numerical methods. This approach to specifying the boundary conditions can be used not only when attached shocks but also centered expansion waves are formed on the leading edges of a wing.

The impermeability condition on the wing surface is satisfied by means of correcting the velocity vector after any integration step by discarding the normal component of the vector.

The problem is solved by time integration on the basis of the explicit McCormack scheme until the steady state is attained. To suppress oscillations on the shock fronts the smoothing procedure of the type of artificial viscosity is introduced. It can conveniently be represented in the form:

$$\mathbf{U}_i = (1 - 2\varepsilon)\mathbf{U}_i + \varepsilon(\mathbf{U}_{i-1} + \mathbf{U}_{i+1}),$$

where ε is a small parameter. For a gridpoint on the wall we have

$$\mathbf{U}_1 = (1 - 2\varepsilon)\mathbf{U}_1 + 2\varepsilon\mathbf{U}_2.$$

The second-order approximation turned out to be necessary, since in the transitional regimes from the symmetric flow with several critical points in the shock layer to flow at yaw [6] the accuracy of the first-order schemes is insufficient.

Table 1

N	1	2	3	4	5
γ, deg	80	40	120	120	120
β, deg	45	45	90	75	60

2. RESULTS OF THE CALCULATIONS OF THE M = 3 FLOW PAST UNYAWED WINGS

Here, we present certain results of the calculations of flows past wings at the freestream Mach number M = 3 and the geometrical parameters given in Table 1. All the calculations were performed at the same difference scheme parameters on the grids with $n = 800$ and 1600 gridpoints on any panel. The data on the flow structure are chiefly presented by the numbered pressure contours (pressure ratio to that in the undisturbed flow) and the streamlines (lines with arrows).

In Fig. 2 we have presented the results of the calculations of symmetric flow around wing 1 (Table 1) which make it possible to trace the transformation of the flow structure in the shock layer, as the angle of attack α varies from 15.75 to 33°. The full flow patterns in the region bounded by the bridge-shaped and internal shocks of the Mach-type shock configuration are supplemented with the enlarged fragments of the flow pattern in the vicinity of the axis of symmetry which contain the described special features of the flow structure.

At low angles of attack the classical streamline pattern is observable, when all the streamlines arrive at a node located at the bend point of the transverse wing contour (is not presented). Further on ($\alpha < 16°$) the streamlines proceeding from the branching points of the Mach-type shock configuration form a "beak" in which all streamlines that have passed across the bridge-shaped shock of the Mach-type configuration find themselves, and end at the wing contour bend point (Fig. 2a). With further increase in the angle of attack on the ranges from 16.25° to 17° (Fig. 2b) and from 17° to 33° (Fig. 2c–2e) the flow is qualitatively restructured. Two more critical points appear in the plane of symmetry. The lower point located nearer to the bend in the contour is the divergence point for certain streamlines that have passed across the shocks attached to the leading edges and the internal shocks of the Mach-type shock configuration. The upper point is at first the node-type Ferri singularity for all the streamlines that have passed through the Mach-type shock system above the streamlines arriving at the lower divergence point (Fig. 2b) and then it becomes a saddle point (Fig. 2c–2e). In the latter case two flows streaming from below, from the divergence point, and from above, from the bridge-shaped shock, form a critical point (Ferri singularity), together with two contact discontinuities proceeding from it on either side of the plane of symmetry and rolling together with other streamlines into two vortex Ferri singularities. The appearance of two more critical points on the axis of symmetry of the flow at a certain angle of attack and then of two vortex Ferri singularities at the vertices of the contact discontinuities proceeding from the upper critical point of the saddle type is precisely the essence of the phenomenon called the Ferri point floating on the windward side of a V-wing in the presence of the Mach-type shock configuration, another than the treatment of the calculated results in [1, 2].

In the case presented in Fig. 2e the calculation of the branching points on the bow shock shows that the internal shock belongs to the weak family, which is indicated by the diagram of the interaction between the shock polars in Fig. 3a. In Fig. 3 the fragments of the flow in the vicinity of the right branching point (Fig. 2e) are presented, together with the pressure (a) and Mach number (b) contours. An analysis shows that in the flow regime under consideration the internal shock cannot have its own branching point. For this reason, the supersonic region downstream of this shock is most probably closed by a submerging shock "resting" by its ends with zero intensities upon the contact discontinuity proceeding from the corresponding branching point on the bow shock, on one hand, and on the internal shock at the point in which the sonic velocity on the sphere is reached, on the other hand.

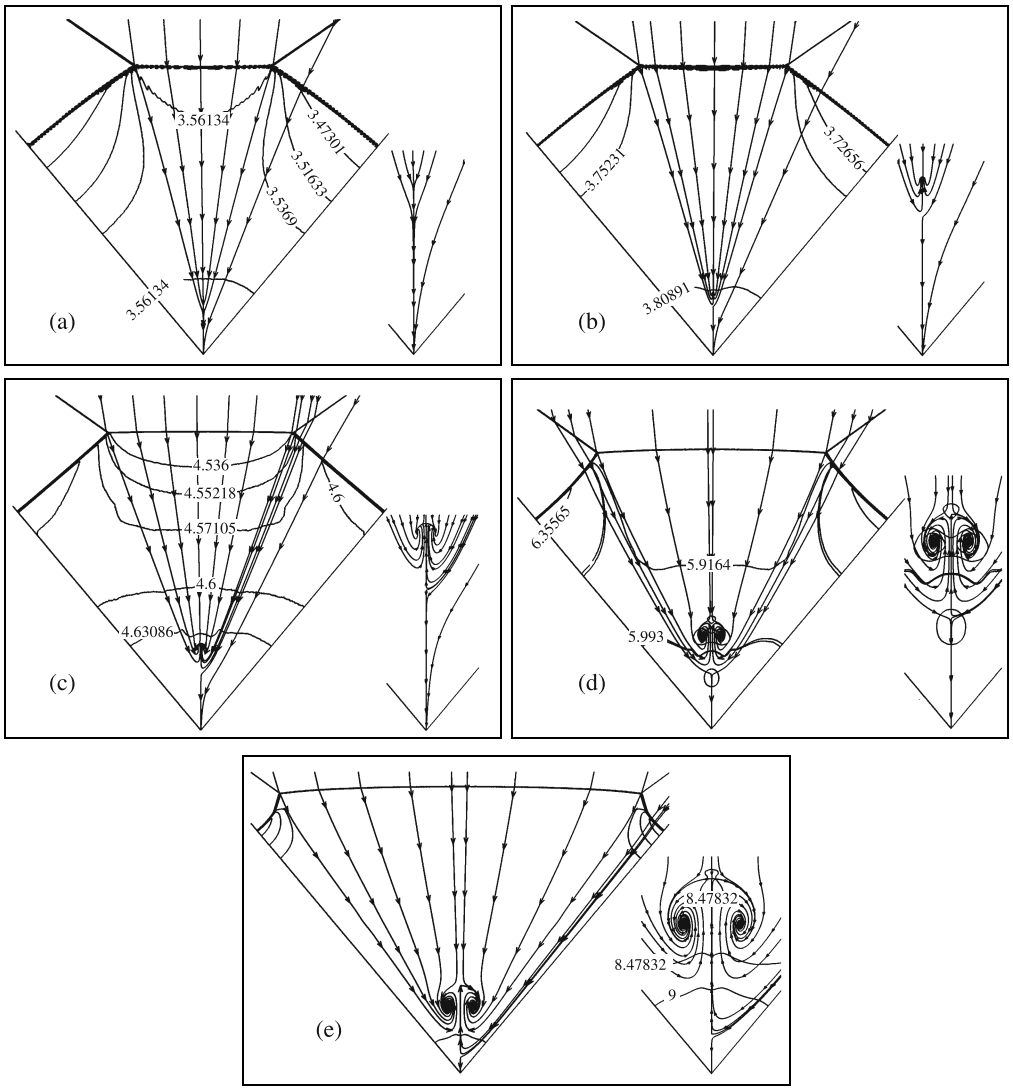

Fig. 2. Symmetric M = 3 flow around the wing with $\gamma = 80^\circ$ and $\beta = 45^\circ$ at the angles of attack $\alpha = 15.75$ (a), 16.75 (b), 20 (c), 25 (d), and 33° (e) (pressure contours and streamlines).

Figure 4 presents the arrangement of the new critical points in the plane of symmetry relative to the point of bend in the transverse contour. The descending regions of the curves are realized approximately with transition of the internal shock to the weak family at the interaction point. For the wing of the geometry under consideration at M = 3, in accordance with the accurate calculations of the branching point on the bow shock, this transition is realized at an angle of attack $\alpha \approx 29^\circ$. The calculations used the Mach number of the freestream velocity component normal to the ray of the conical coordinate system passing through the branching point, whose coordinates are determined from the results of numerical calculations, and the intensity of the shock attached to the leading edge.

We note that, in accordance with the calculations, the pressure at the branching point in the internal flow region at relatively small angles of attack is higher than the pressure on the wing wall directly behind the internal shock normally incident on the wall; however, the relationship between these characteristic pressures changes with increase in the angle of attack. The intersection of the angle-of-attack–pressure curves at these points is realized at $\alpha \approx 20^\circ$ (Fig. 2c). The coordinate α of their intersection approximately indicates the angle of attack at which the convexity of the internal shock changes from the direction toward the leading edge (Fig. 2b) to that toward the central chord of the wing (Fig. 2c and 2d). The change in

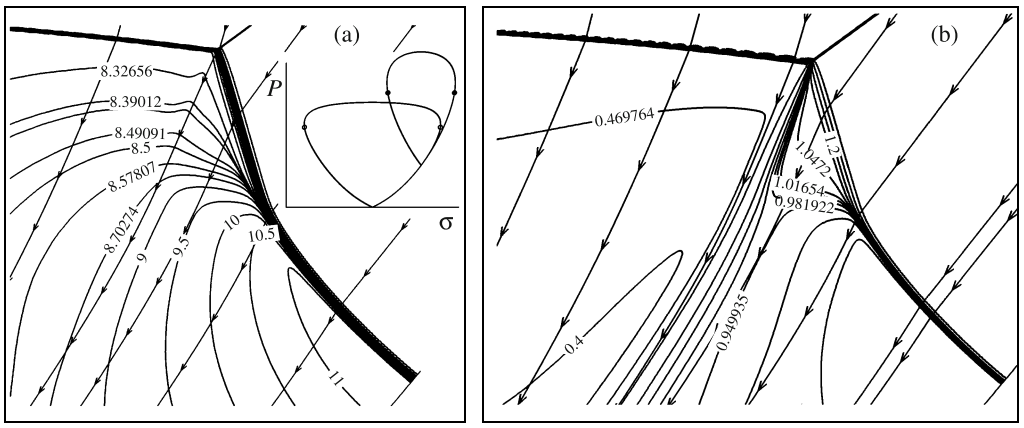

Fig. 3. Fragment of the flow in the vicinity of the right branching point on the bow shock: pressure (a) and Mach number (b) contours on the sphere.

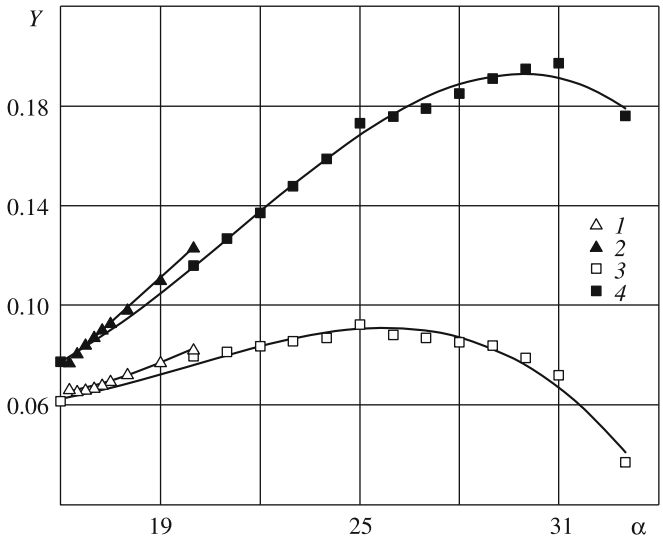

Fig. 4. Position of the critical points in the plane of symmetry of the wing with $\gamma = 80^\circ$ and $\beta = 45^\circ$ relative to the point of bend in the transverse contour; (*1*, *2*) calculations on the $n = 800$ grid and (*3*, *4*) $n = 1600$; (*1*, *3*) relate to the divergence point and (*2*, *4*) to the Ferri singularity.

the convexity direction is realized via the appearance of an inflection point on the internal shock of the Mach-type configuration.

Below we present certain results of the calculations of flow around wing 2 (Table 1) with a fairly small angle of vee $\gamma = 40^\circ$. For this wing the flow patterns realized at M = 3 can involve both regular and Mach-type reflections of the plane shocks attached to the leading edges from the plane of symmetry. In the case of the regular interaction flow past an "internal" wing with the leading edge at the point of the plane shock arrival onto the plane of symmetry was calculated. For this wing the undisturbed flow is the uniform flow behind the shock attached to the leading edge. A fragment of the corresponding flow structure containing two additional critical points in the plane of symmetry (which is a wall for the main wing), of which the upper point, or the Ferri singularity of the node type, corresponds to the angle of attack of the main wing $\alpha = 21^\circ$, is presented in Fig. 5a. This result was obtained on the $n = 1600$ grid.

Figure 5b illustrates the regime of the flow around the original wing at $\alpha = 23.8^\circ$ corresponding to the exact solution with a plane shock reflected from the plane of symmetry and belonging to the strong family in the plane normal to the corresponding conical ray (reflection line) [7]. Here, the numerical realization of the exact solution is presented.

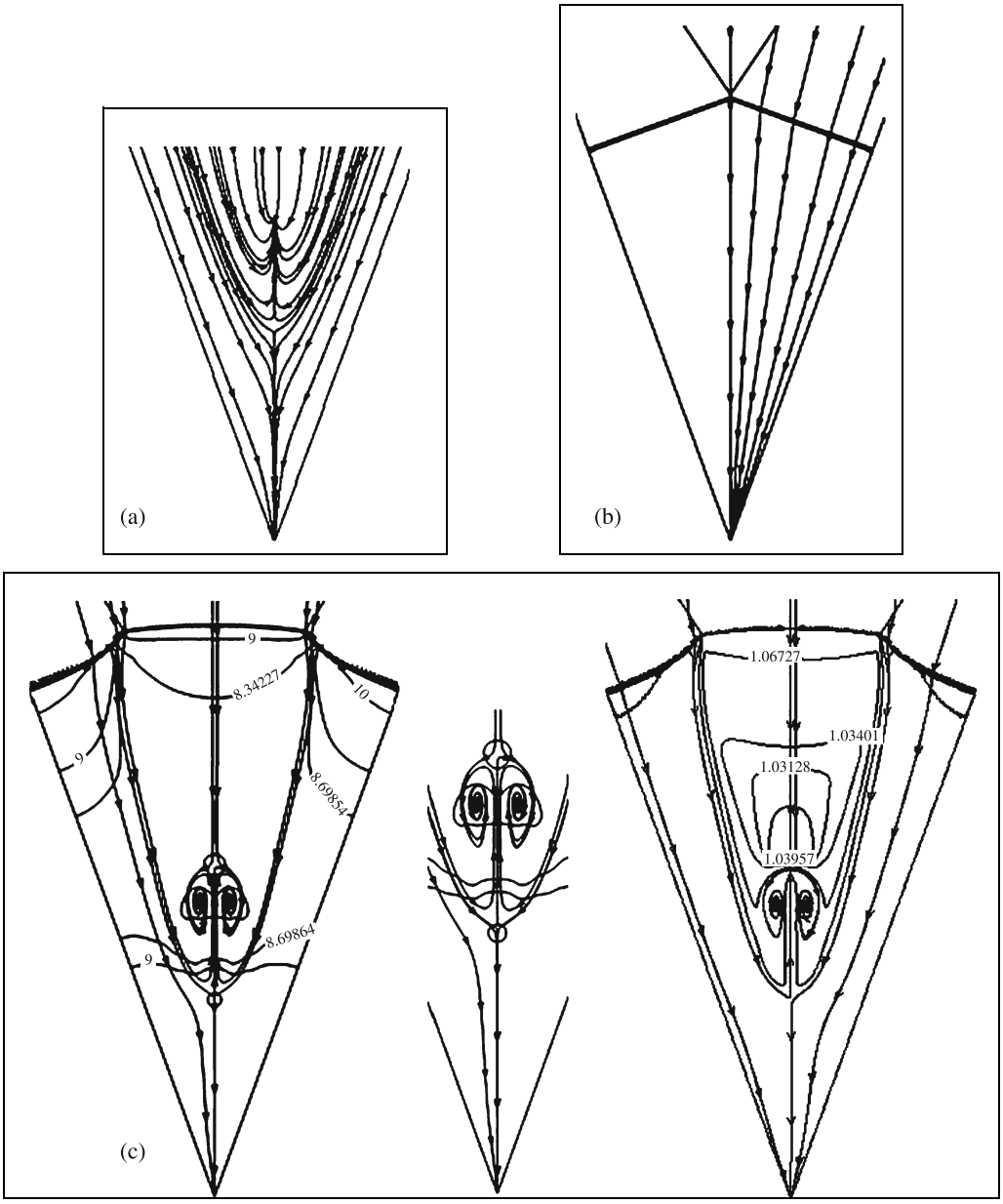

Fig. 5. Symmetric M = 3 flow around the wing with $\gamma = 40^\circ$ and $\beta = 45^\circ$ at the angles of attack $\alpha = 21^\circ$ (a), $\alpha = 23.8^\circ$ (exact solution with the plane strong-family shock reflected from the plane of symmetry) (b), and $\alpha = 32^\circ$ (pressure contours, streamlines, and contours of the Mach number based on the total velocity) (c).

In Fig. 6 we have plotted the dependences of the pressure on the angle of attack at three characteristic points of the disturbed region. The first is located downstream, at the point of branching of the shock reflected from the plane of symmetry (curve *1*, $\alpha < 23.8^\circ$). The second is on the wing wall (curve *2*) behind the bridge-shaped shock of the Mach-type shock configuration, near the "internal" wing ($\alpha < 23.8^\circ$) and behind the internal shock near the main wing ($\alpha > 23.8^\circ$). The third point is behind the branching point of the Mach-type shock configuration near the main wing (curve *3*, $\alpha > 23.8^\circ$). In the same diagrams of the flow around the wing the characteristic points numbered in accordance with the numbers of the curves are presented. The vertical segment of the broken line corresponds to $\alpha = 23.8^\circ$, that is, the boundary of transition from the regular to the Mach-type interaction between the shocks attached to the leading edges of the wing. Clearly that in the on-design flow regime (exact solution, Fig. 5b) the pressure level behind the internal shock I belonging to the strong family coincides with that on the wall (curve *2*, Fig. 6) at $\alpha = 23.8^\circ$.

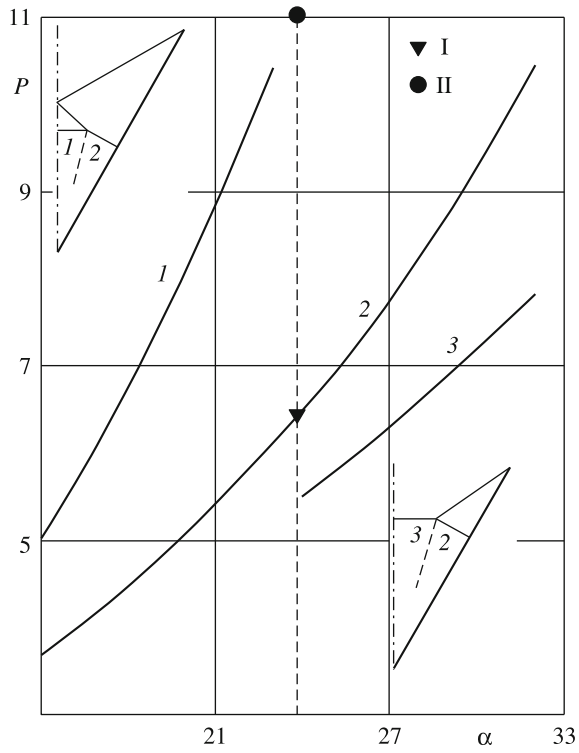

Fig. 6. Angle-of-attack-dependence of the pressure at three characteristic points of the disturbed region; (*1*) at the branching point of the shock reflected from the plane of symmetry; (*2*) on the wing wall; and (*3*), behind the point of branching of the Mach-type shock configuration; I is the pressure behind the internal shock and II is the exact value of the pressure approached by the pressure at point (*1*).

This property of the pressure behind the bridge-shaped shock of the Mach-type shock configuration near a V-wing was established in [8] at the passage to the limit $\alpha \to \alpha_c$ from below. Here, α_c is the angle of attack corresponding to the on-design flow regime with a leading-edge shock belonging to the strong family.

We note that downstream of the branching point of the shock the pressure near the internal wing (Fig. 6, curve *1*) is much higher that pressure I, as the angle of attack approaches from below the angle of attack corresponding to the exact solution (II is the accurately calculated pressure level approached by the pressure at the above-mentioned characteristic point). This means that in the vicinity of the branching point in the shock layer there exists an elevated-pressure region with respect to the pressure at the center of the bridge-shaped shock, while the normal force acting in this case on the wall of the "internal" wing, suffers a discontinuity as the on-design flow regime is reached. This fact was noticed before in [2].

In Fig. 5c we have presented the flow structure near the wing under consideration with the pressure contours and streamlines, its enlarged fragment in the vicinity of the plane of symmetry of the flow containing the critical points and the vortex Ferri singularities, and the flow structure with the Mach number contours and streamlines at $\alpha = 32^\circ$. These data pertain to a flow regime which is close to the breakdown of the conical flow near a finite-length wing due to the passage of the total flow velocity in the upper vicinity of the floating Ferri singularity (upper critical point in Fig. 5c) through the speed of sound [1]. In this case, the total velocity in this vicinity differs from the critical velocity by less than 3%. We also note that, as in the case of flow around wing 1 (Table 1), in the vicinity of the branching points under the contact discontinuity the Mach number based on the flow component on the sphere becomes greater than unity at $\alpha \approx 29^\circ$. Thus, in this case (Fig. 5c) downstream of the branching point under the contact discontinuity there is supersonic flow on the sphere, which is in agreement with the internal shock shape and the structure of the pressure contours.

In Fig. 7 the data on the moment of appearance and the position of the critical points for wing 3 (Table 1)

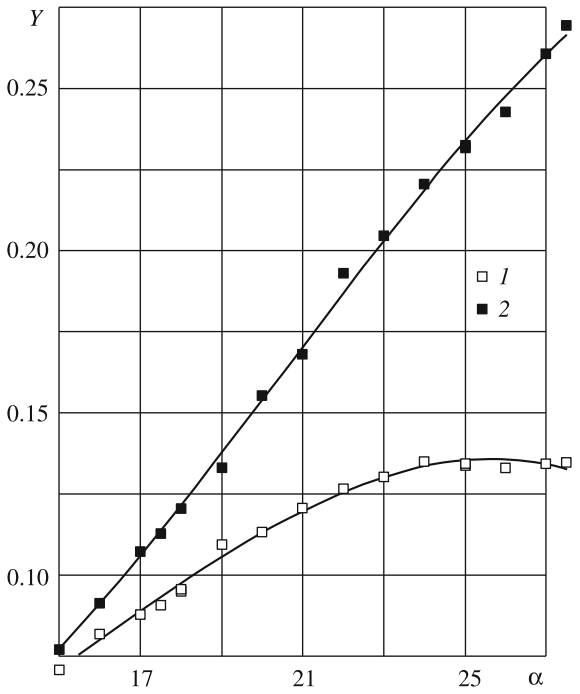

Fig. 7. Position of the critical points in the plane of symmetry of the wing with $\gamma = 120^\circ$ and $\beta = 90^\circ$ relative to the point of bend in the transverse contour; (*1*) is the divergence point and (*2*) is the Ferri singularity.

are presented; these were obtained on the $n = 1600$ grid. On the angle-of-attack range considered there are no wing flow regimes with supersonic flow beneath the contact discontinuity at the branching point. The critical velocity is reached only at $\alpha \approx 27.5^\circ$. Apparently, by virtue of this fact, the curves describing the position of the critical points in the plane of symmetry have no descending regions (Fig. 7), as distinct from the corresponding dependences for wing 1 (Table 1 and Fig. 4).

3. RESULTS OF THE CALCULATIONS OF FLOW AROUND A YAWED WING AT M = 3. COMPARISON WITH THE EXPERIMENTAL DATA

In this section we present the results of the calculations of flow around wing 3 (Table 1) which allow one to make conclusions about the restructuring of the shock-layer flow pattern containing three critical points in the plane of symmetry and two vortex Ferri singularities in flow at the angle $\vartheta = 0$ (Fig. 1a) with increase in the yaw angle and their comparison with the experimental data obtained using the optical method [5].

In Fig. 8 the variation in the flow structure in the compressed layer near wing 3 with increase in the angle of yaw ϑ is shown at the angle of attack $\alpha = 25^\circ$. The Mach-type shock configuration (pressure contours) and streamlines (arrowed curves) are presented. We note that in the first three flow regimes (Fig. 8a–8c), the contact discontinuity proceeding from the left branching point enters into the left vortex Ferri singularity, while the contact discontinuity proceeding from the branching point enters into the right vortex singularity. In the layer there are two critical points of the saddle type and a vortex Ferri singularity of the node type on the right panel. With increase in the angle of yaw (Fig. 8d), when the streamlines neighboring the contact discontinuity proceeding from the left branching point (or the contact discontinuity itself) do not enter in the number of the streamlines forming the left vortex Ferri singularity, a new vortex singularity is formed above the right panel surface, while the upper left vortex singularity becomes less clearly expressed.

Figure 9 presents the fragments of the shock-layer flow structure at the same angle of attack with further increase in the angle of yaw ϑ. The color shades illustrate the pressure variation. According to the results of the calculations the upper vortex Ferri singularities vanish at $\vartheta \approx 14^\circ$ and at $\vartheta \approx 15^\circ$ only one vortex Ferri singularity in the vicinity of the right wing panel can be observable (Fig. 9d).

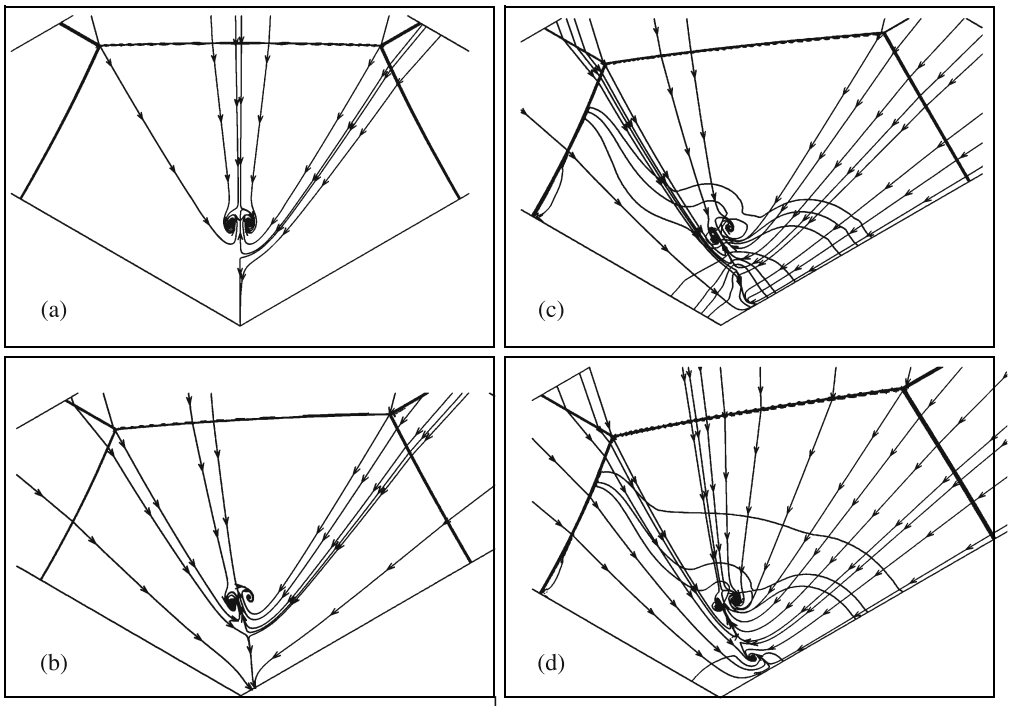

Fig. 8. Flow structures in the compressed layer on the wing with $\gamma = 120^\circ$ and $\beta = 90^\circ$ at M = 3 and the angles of attack $\alpha = 25^\circ$ and yaw $\vartheta = 0$ (a), 2 (b), 4 (c), and 6° (d).

In Fig. 10 we have presented the experimental data on the optical investigation of the flow structure on wing 3 and compared them with the results of the calculations within the framework of the inviscid gas model (Section 2). In Fig. 10a the representative points of the experimental regimes reviewed in Table 2 are shown in the $(\vartheta,\ \alpha)$ plane.

In the same figure curves (*1–4*) corresponding to the boundaries of the parameter ranges with different wing flow regimes are plotted for M = 3. Curve *1* corresponds to transition from the shock to the shockless flow in the layer above the right wing panel, *2* to transition from the attached shock to a centered expansion wave on the leading edge of the left panel, *3* to unconditional transition from the regular to the Mach-type interaction between the shocks proceeding from the leading edges, and *4* to the shock detachment from the leading edge of the right panel [6]. The grid of the other numbered curves corresponds to different intensities of the internal shock on the left panel wall. We note first that at the intensity $p = 1.6$ of the shock incident on the wall turbulent boundary layer separation starts to form [9]. It becomes developed at $p \approx 2.5$ and higher.

In accordance with the terminology adopted, in these cases the λ shock configuration accompanying boundary layer separation is clearly observable and the contact discontinuity proceeding from the corresponding branching point is visible in the shadowgraphs. Clearly that the difference in the flow structure, compared with the data of the calculations within the framework of the inviscid gas model, might be expected only at the three upper representative points (particularly, at the right representative point). In the presence of a positive yaw angle (Fig. 1a) the internal shock intensity is higher on the left panel of the wing under consideration than on the right panel. Thus, at $\vartheta > 0$ turbulent boundary layer separation is first generated on the left panel. In these cases, the calculated and experimental results will be compared only for the flow structures in the shock layer above the right panel of the wing.

In the combinations of the shadowgraphs and calculated data obtained for cases 1 and 2 of Table 2 (Fig. 10b and 10c) it can be seen that boundary layer separation is absent and only its thickening is visible, which is due to the action of the shocks incident on the wall whose shapes are distorted in the vicinity of the wall as a result of the interaction with the boundary layer. However, this has no effect on the flow in the vicinity of the plane of symmetry of the wing. The flow structures are in complete agreement.

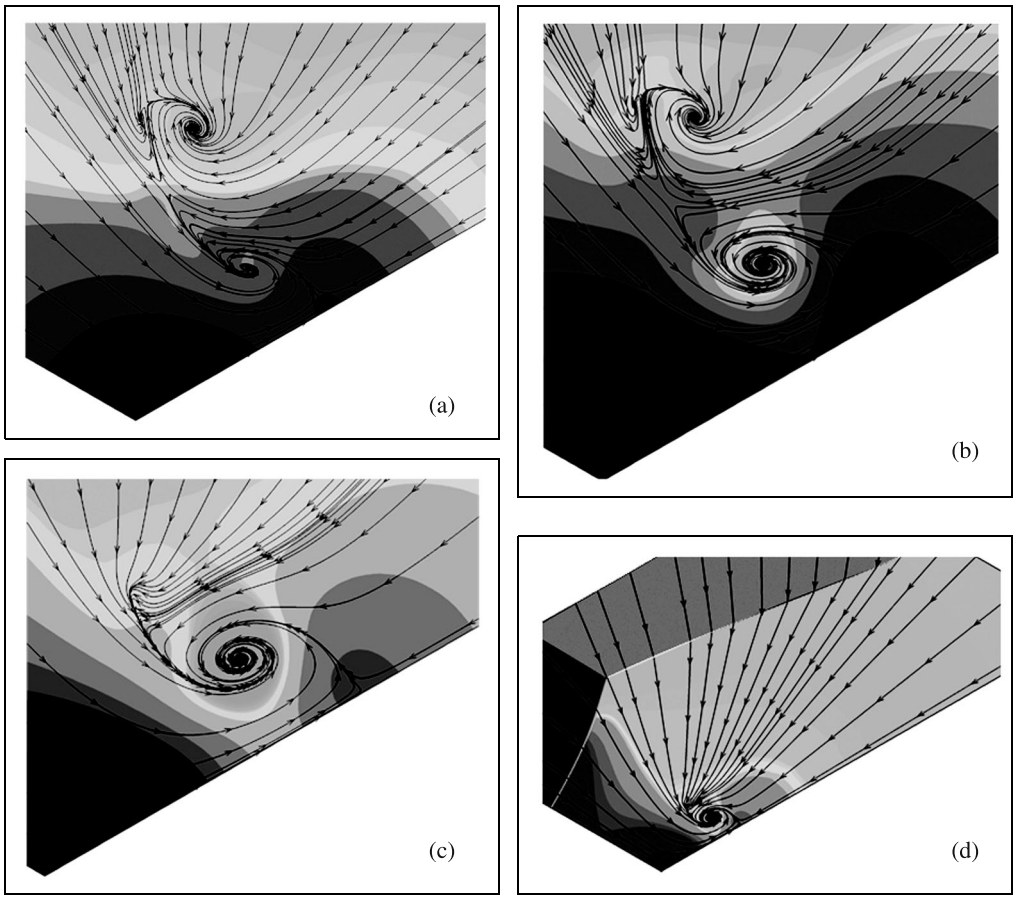

Fig. 9. Fragments of the flow in the shock layer on the wing with $\gamma = 120^\circ$ and $\beta = 90^\circ$ at M = 3 and the angles of attack $\alpha = 25^\circ$ and yaw $\vartheta = 8$ (a), 10 (b), 14 (c), and 15° (d).

Table 2

N	1	2	3	4	5	6
α, deg	15	20	20	25	25	22.1
ϑ, deg	0	0	5	1	6	17.6

In Fig. 10d–10g, we have presented the flow patterns, of which the first three pertain to the range of insufficiently developed separation of the turbulent boundary layer (cases 3 to 5 in Table 2). Only the last flow pattern (case 6 in Table 2) can be associated with the parameter range with developed separation. However, even in this flow regime, despite the presence of boundary layer separation from the left panel, any visible differences between the experimental and calculated flow structures in the shock layer on the right wing panel cannot be observable on this parameter range. On the left panel the separation has only a local effect.

Thus, the results of the calculations within the framework of the Euler model quite adequately reproduce the salient features of the actual shock-layer flow structure in the regimes of transition from the symmetric to nonsymmetric flow around V-wings if only the intensity of the contact discontinuity generated by the λ shock configuration is not comparable with (or greater than) the intensity of the contact discontinuities proceeding from the branching points of the bow shock [6].

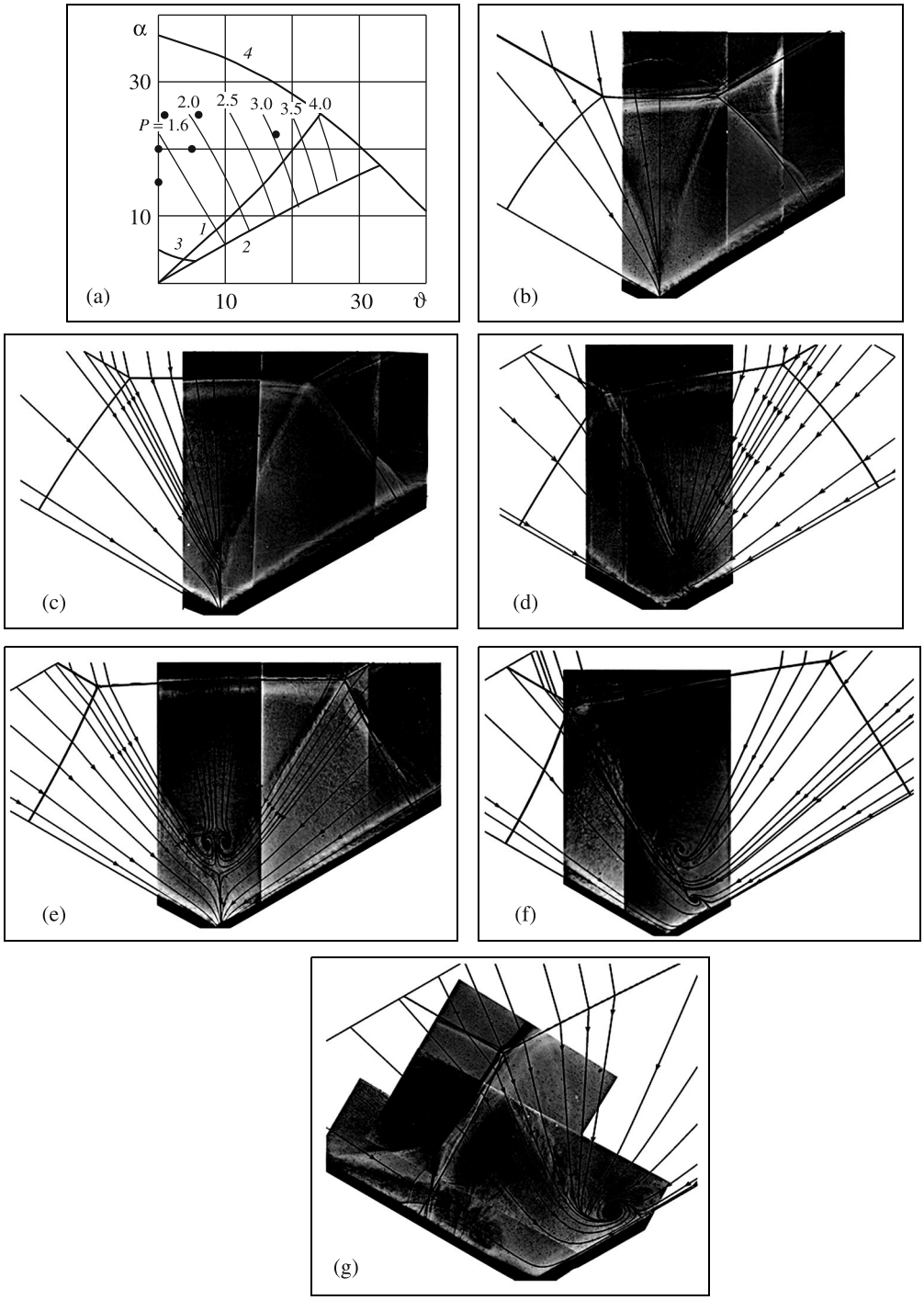

Fig. 10. Ranges of existence of different flow regimes for the wing with $\gamma = 120^\circ$ and $\beta = 90^\circ$ at M = 3 and the representative points of the experimental regimes (b–g, see Table 2) (a) and flow shadowgraphs and data of calculations (pressure contours and streamlines) in the above-noted regimes.

4. CONDITION OF THE EXISTENCE OF THE VORTEX FERRI SINGULARITIES

The question of the reasons for the Ferri singularity floating on the windward side of a V-wing was formulated in [1]. In that study this phenomenon was attributed to large losses of the total pressure in the normal shock (bridge-shaped shock in the Mach-type shock configuration) as compared with the losses in the system of oblique and normal shocks (shock on the leading edge and internal shock in the vicinity of the wing wall). The data on the existence of the vortex Ferri singularities were absent. Later, with increasing possibilities of the computational technologies, the vortex Ferri singularities were detected. Their appearance and disappearance was attributable to the intensity of the generating contact discontinuities [10, 11], since on the boundary of the elliptic region of the conical inviscid-gas flow there are no singularities other than the contact discontinuities proceeding from the branching points on the bow shock.

In the actual flow boundary layer separation from the wing panels develops at a sufficient intensity of the internal shocks. In these cases, on the boundary of the elliptic region (internal relative to the shock waves and Mach cones) there appear new singularities due to the contact discontinuities generated by λ shock configurations above the boundary layer separation zone. Depending on the relation between the contact discontinuity intensities, on the boundary of the elliptic region of the conical flow new singularities in the shock-layer flow structure, as compared with those in an inviscid gas, can arise, including new vortex Ferri singularities [6].

For the wings, whose geometric parameters are given in Table 1, it is the quantity ΔK used in [6, 10, 11] that was chosen as the contact discontinuity intensity: $\Delta K = (K_1 - K_2)/K_1$, $K = S^k$, $k = 1/(1 - \kappa)$. Here, K is the total pressure recovery coefficient determined in terms of the entropy function S, κ in the specific heat ratio, and K_1 and K_2 are the total pressure recovery coefficients calculated on the either side of the contact discontinuity proceeding from the branching point on the bow shock in the Mach-type shock configuration, K_1 corresponding to the gas particles which have passed across two shocks in the three-shock configuration and K_2 to those that have passed across only one shock. The quantity ΔK is determined as a result of the accurate calculation of the branching points using their coordinates obtained from the numerical calculation data and is based on the Mach number M_n of the undisturbed flow velocity component normal to the ray of the conical coordinate system passing through the branching point and the intensity of the shock attached to the leading edge.

In Fig. 11 curves (*1–5*) present the $\Delta K(\alpha)$ dependences for wings 1 to 5 (Table 1) in $M = 3$ flow without yaw. For wing 2 the data are presented for $\alpha > 23.8^\circ$, when the Mach-type shock configuration occurs near the wing. The bends in curves *4* and *5* at certain values of α are due to different structures of the branching points. At the angles of attack smaller than those corresponding to the bends in the $\Delta K(\alpha)$ curves plotted in Fig 11 the branching point structure includes, apart from the shocks, a centered expansion wave which vanishes, when the values of α become greater than the coordinates of the bend points. Since the step in the angle of attack at which the numerical calculations were conducted, was not less than 0.25°, the data I and II have a corresponding error.

As follows from an analysis of the theoretical and experimental data presented above, the vortex structures (vortex Ferri singularities [6, 10, 11]) in the shock layer are formed by contact discontinuities and the neighboring streamlines, while their "intensity" (Figs. 2 and 8–10) depends on the intensity of the corresponding contact discontinuity which is characterized here by the quantity ΔK.

According to the calculations, the intensity of the contact discontinuity proceeding from the left branching point on the bow shock of wing 3 (Table 1) vanishes at $\alpha < 17.5^\circ$, when the representative point of the regime approaches curve *2* (Fig. 10a), at which the disturbance produced by the left panel is zero. In this case, the vortex Ferri singularity located above the right panel surface (Fig. 9d) descends on the wall and is no longer of the vortex-type transforming in the streamline node. This occurs at $\Delta K \approx 0.15$ [11]. At large angles of attack, when an increase in the yaw angle does not lead the representative point of the regime to curve *2* (Fig. 10a), the vortex Ferri singularity remains within the shock layer above the right panel, only changing its intensity and the distance from the wall. It should be added that in flow around the wing under

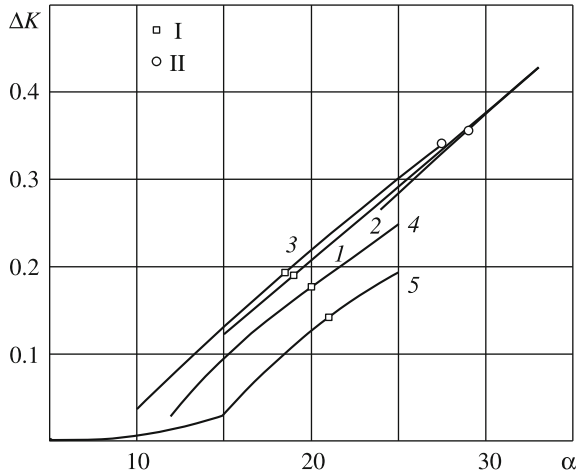

Fig. 11. Intensities of the contact discontinuities proceeding from the branching points on the bow shock as functions of α for wings 1 to 5 (Table 1) in M = 3 flow without yaw; I relate to the values of ΔK at which the vortex Ferri singularities are realized in the shock layer on the wing on either side of the plane of symmetry of the flow and II are the points at which the velocity on the sphere is critical at the branching points.

consideration at the angles of attack $\alpha < 14^\circ$, when the contact discontinuity intensity $\Delta K < 0.15$, the vortex Ferri singularities are not formed in the shock layer [11].

Together with the data presented in Fig. 11, the data presented above allow us to suppose that there exists a certain minimum "threshold" value $\Delta K^* \approx 0.15$ such that the contact discontinuity cannot generate any vortex singularity if its intensity is less than ΔK^*.

We will now compare the data on flow around wing 3 (Section 3, Figs. 8 and 9) with the inference made above. In the wing flow regimes presented in Fig. 8 the intensity of the contact discontinuities proceeding from the left and right branching points is considerably greater than ΔK^* ($\Delta K \approx 0.3$). Because of this, at the yaw angle $\vartheta = 6^\circ$ (Fig. 8d) the near-wall right and upper vortex Ferri singularities formed by the above-mentioned contact discontinuities are clearly expressed objects in the shock layer. With increase in the yaw angle the intensity of the contact discontinuity proceeding from the right branching point decreases and becomes less than ΔK^* at $\vartheta \approx 14^\circ$. The upper vortex Ferri singularity disappears (Fig. 9c). At the same time, the intensity of the left contact discontinuity, which forms the vortex Ferri singularity above the right panel surface, increases and reaches its maximum value $\Delta K \approx 0.4$ at $\vartheta = 15^\circ$. In this case, a single clearly expressed vortex Ferri singularity is observed in the shock layer above the right panel surface (Fig. 9d).

Thus, the analysis made above indicates that at M = 3 the condition $\Delta K^* \approx 0.15$ performs well in determining the appearance and disappearance of vortex Ferri singularities in the shock layers of conical flows. The question of the applicability of this criterion at other Mach numbers calls for further investigation.

Summary. A comprehensive theoretical and experimental investigation of the flow structure in the shock layers on a set of V-wings in M = 3 flow at angles of attack and yaw with shocks attached to the leading edges is made.

It is shown the flow structure in the plane of symmetry near the V-wings in flow without a yaw angle undergoes a jumpwise change with increase in the angle of attack, when the Mach-type shock configuration is realized. In addition to one Ferri singularity of the node type located at the bend point on the transverse wing contour, two more critical points, those of divergence and convergence (second Ferri singularity) appear in the plane of symmetry of the flow, where they are located near the bridge-shaped shock of the Mach-type shock configuration. The latter point can be of both the node and the saddle type. In the latter case vortex Ferri singularities are located at the vertices of the contact discontinuities proceeding from the critical point on either side of the plane of symmetry. The flow restructuring with increase in the yaw angle is considered.

It is established, in particular, that the shock-layer flow structure containing the three above-mentioned critical points and the two vortex Ferri singularities goes over into a structure having a critical point at the wing contour bend, namely, the flow convergence point or the Ferri singularity on the windward panel, into which the streamlines proceeding from the leading edges enter, and the vortex singularity located above the panel surface, at the vertex of the contact discontinuity proceeding from the Ferri singularity on the wing wall.

It is shown that, as concerns the generation and development of the flow structures containing the vortex Ferri singularities, the results of the calculations within the framework of the inviscid gas model are in good agreement with the experimental data on the optical flow visualization in the plane normal to the central chord of the wing over a wide range of the angles of attack of yaw.

It is shown that the appearance and disappearance of the vortex Ferri singularities is governed by the intensities of the contact discontinuities that form these singularities. It is established that there exists a threshold minimum value of the parameter characterizing the contact discontinuity intensity equal to approximately 0.15 at the freestream Mach number $M = 3$. If the intensity of the contact discontinuity on the boundary of the internal disturbed region of the conical flow is less than this value, than the corresponding contact discontinuity is not able to generate a vortex Ferri singularity.

The study was carried out with the support of the Russian Foundation for Basic Research (project No. 12-01-343a). The calculations were performed on a supercomputer of the Russian Academy of Sciences.

REFERENCES

1. N.A. Ostapenko, "On the Floating of the Ferri Point on the Windward Side of a V-Wing," Dokl. Akad. Nauk SSSR **287**, 295 (1986).
2. M.A. Zubin and N.A. Ostapenko, "The Flow Structure near the Windward Side of V-Shaped Wings with an Attached Shock Wave on the Leading Edges," Fluid Dynamics **21** (1), 104 (1986).
3. Yu.P. Gun'ko, A.N. Kudryavtsev, and R.D. Rakhimov, "Supersonic Inviscid Corner Flows with Regular and Irregular Shock Interaction," Fluid Dynamics **39** (2), 304 (2004).
4. M.A. Zubin, F.A. Maksimov, and N.A. Ostapenko, "On Certain Properties of the Flow Structure in the Shock Layers on V-Wings at Yaw Angle," in: *Proc. XII Int. School-Workshop 'Models and Methods in Aerodynamics'* [in Russian], Moscow (2012), p. 94.
5. A.L. Gonor, M.A. Zubin, and N.A. Ostapenko, "Use of Lasers in Experimental Aerodynamics," in *Instrument and Automatized Control. No. 2* [in Russian], Mashinostroenie, Moscow (1985), p. 5.
6. M.A. Zubin, N.A. Ostapenko, and A.A. Chulkov, "Conical Gas Flows with Shock Waves and Turbulent Boundary Layer Separation," Fluid Dynamics **47** (2), 263 (2012).
7. N.A. Ostapenko, "Regimes of Supersonic Flow around V-Wings," Tr. MIAN **223**, 238 (1998).
8. V.I. Lapygin, "Solution of the Problem of the Flow around a V-Shaped Wing with a Strong Shock at the Leading Edge," Fluid Dynamics **8** (3), 439 (1973).
9. M.A. Zubin and N.A. Ostapenko, "Geometric Characteristics of the Separation of a Turbulent Boundary Layer in the Case of Interaction with a Normal Shock Wave in Conical Flows," Fluid Dynamics **18** (6), 867 (1983).
10. M.A. Zubin, N.A. Ostapenko, and A.A. Chulkov, "On a Singularity of Conical Gas Flows with Shocks and Boundary Layer Separation," Dokl. Ross. Akad. Nauk **404**, 339 (2005).
11. M.A. Zubin, N.A. Ostapenko, and A.A. Chulkov, "Structure of Supersonic Nonsymmetric Conical Flow around a V-Wing," Fluid Dynamics **46** (4), 634 (2011).